A comprehensive study of simulated cyclic indentation response of linear viscoelastic materials

Olga Smerdova

A comprehensive study of simulated cyclic indentation response of linear viscoelastic materials

Olga Smerdova

Institut Pprime, CNRS, ISAE-ENSMA, Université de Poitiers, Futuroscope Chasseneuil F-86962, France

olga.smerdova@ensma.fr

Full postal address: ISAE-ENSMA, 1 av. Clément Ader, Chasseneuil du Poitou 86360, France

Abstract

This paper presents and analyzes the cyclic indentation response of a linear viscoelastic material over the entire time range of the relaxation processes using conical or spherical indenters. Finite Element simulations of cyclic indentation on two Generalized Maxwell materials with different relaxation spectra were performed. A variety of cyclic responses to indentation were generated and analyzed using an analytical method based on elastic contact. It is shown that the elastic contact depth and contact stiffness from the loading curves should be used to identify the relaxation modulus corresponding to the time of loading. The stabilization of the loop has also been studied through the energy ratio, a parameter that describes the evolution of the dissipated energy with cycles. A simple time shift between cyclic creep and monotonous indentation creep of a linear viscoelastic material is demonstrated. The simulated indentation curves and the parameters derived from them were found to be qualitatively similar to the experimental cyclic indentation data on HDPE polymer at different loading rates. Assuming that the first loading is affected by plasticity due to the use of a sharp indenter, a correction was suggested to obtain the elastic relaxation modulus from the experiments. The values of the modulus identified in this way for HDPE compared well with the relaxation modulus identified for this material from previous cyclic tensile experiments. The small discrepancy was attributed to the non-linear viscoelasticity or the viscoplasticity of the polymer.

Keywords:

Linear viscoelasticity, instrumented indentation, finite element simulations, cyclic loading, indentation creep, polymer

1. Introduction

The use of instrumented indentation, or nanoindentation, as an experimental technique to explore the mechanical behavior of materials has been steadily growing over the last thirty years. It is employed across a wide range of materials, from metals to polymers, ceramics, and glasses. Its ability to probe the mechanical response of a volume of only several microns makes it irreplaceable for measuring the local properties of heterogeneous materials, such as polymer composites [1-4]. The force-displacement response of a polymer to penetration by a rigid tip of known shape is usually analyzed using analytical models [5, 6] or employed in numerical identification procedures through inverse methods [7, 8] to obtain the parameters of a chosen constitutive law. The advantage of the former is its simplicity in manipulation, while the latter can describe more complex behaviors and are useful for parametric studies.

The standard analysis method implemented in all nanoindentation software is the one suggested by Oliver and Pharr [5]. This method was developed for metallic materials and provides the elastic modulus and hardness. In contrast, polymers demonstrate time-dependent behavior, which can be described by viscoelastic or viscoelastic-plastic laws. This behavior has been extensively documented in indentation experiments by studying indentation creep [9-11] or rate dependence [12]. The time-dependent response can also be probed through dynamic nanoindentation tests, in which oscillating loading with small amplitude and analysis are similar to Dynamic Mechanical Analysis [13-14]. However, to this day, there is no standard procedure to characterize polymeric materials using a nanoindentation experiment.

The analytical solution for the indentation of a homogeneous isotropic linear viscoelastic material with a rigid spherical indenter was first developed from the elastic solution by Lee and Radok using a method of functional equations [15]. This solution is limited to the case of a monotonically increasing contact area, which, in practice, means the loading or holding phase of a trapezoidal loading path. The results of Lee and Radok were confirmed by Ting [16] and extended to the viscoelastic solution for a more general case of loading history and the shape of the axisymmetric punch. L. Cheng [17] developed an analytical solution for spherical indentation of a viscoelastic material described by a standard linear solid model. This solution was successfully fitted to the experimental indentation creep and relaxation responses of PS and PVOH polymers. Vandamme and Ulm [18] derived closed-form solutions for several simple linear viscoelastic models under conical indentation using the method of functional equations. This solution is applicable to load-controlled experiments and two loading paths: step loading and trapezoidal loading. Three models were studied: the 3-parameter Maxwell model, the 4-parameter Kelvin-Voigt model, and the 5-parameter combined Kelvin-Voigt-Maxwell model.

Although the method of functional equations provides a solution only for the monotonically increasing contact area, Vandamme and Ulm [18] and Cheng and Cheng [19-21] demonstrated that it can also be applied to the initial unloading due to the retardation of the polymer's response. In particular, Cheng and Cheng [19-21] showed that knowing the Poisson's ratio of the material, it is possible to obtain the instantaneous shear modulus G_0 (or the elastic modulus E_0) from the unloading stiffness of the "converged" unloading curve with a high unloading rate. The Finite Element (FE) simulations on a standard solid material provided a converged unloading curve for three different loading histories (constant loading rate, constant displacement rate, and constant strain rate) with the unloading rate of $v > 0.01\tau_1$, where τ_1 is the relaxation time of the material. The authors also showed that the Oliver & Pharr method of estimating the contact depth is inaccurate for a viscoelastic solid. The measured contact depth was found to be consistent with the elastic solution, corrected by a small coefficient $\alpha = 1.034$ and $\alpha = 1.04$ for the conical and spherical indentations, respectively. The error in the estimation of the contact depth was as high as 45% for the cone and 82% for the sphere under certain loading conditions.

Other methods, such as using a sufficiently long holding period at the maximum load or maximum depth [10, 11], or using a constant strain rate during the loading phase [22, 23], have been suggested and utilized by a number of nanoindentation users. Both protocols aim to decrease the impact of the viscoelasticity on the elastic modulus obtained from the unloading. A combination of the constant strain rate loading with the holding at a constant depth was proposed by Baral et al. [24] to obtain the relaxation spectrum of a polymer. However, comparing the results obtained on PMMA with other experimental data proved to be challenging.

In our previous paper [25], we explored the experimental indentation response to cyclic loading of several polymeric materials. In particular, a High-Density Polyethylene (HDPE), a Polymethylmethacrylate (PMMA), and a PR520 epoxy resin were tested. All of these materials demonstrated pronounced viscoelastic behavior that depended on the loading rate. We suggested the cyclic indentation method as a way to study viscoelasticity at several time scales: the instantaneous elastic modulus was calculated at each cycle, the energy ratio between irreversible and

total work was associated with the time scale of one cycle, and cyclic creep, along with the evolution of elastic modulus and energy ratio with cycles, was associated with the time scale of the entire test. In this way, the viscoelasticity was characterized qualitatively across multiple time scales. Another significant novelty was the evaluation of the instantaneous elastic modulus from the reloading curves instead of unloading. The experimental data demonstrated that reloading better respected the condition of elasticity, which is the underlying hypothesis of the analysis.

The aims of the current work are to explore the multitude of possible nanoindentation cyclic responses of a polymer material over the full range of the relaxation processes, and to suggest a new method for identifying the parameters of a viscoelastic law from the force-displacement curves provided by nanoindentation experiments. This is achieved by using a number of finite element (FE) simulations on two Generalised Maxwell materials with different (artificial) relaxation spectra. Different ratios of the loading time to the maximum relaxation time of the material using conical and spherical tips are explored. To begin, the validity of the Oliver and Pharr procedure and the elastic solution to obtain the contact depth is examined. The difference between the elastic modulus obtained by the Oliver and Pharr procedure and the elastic modulus evaluated from the loading is then demonstrated across the entire range of time. The effect of the unloading rate on the elastic modulus is also evaluated. Finally, the suggested method is applied to the experimental results on HDPE polymer and discussed in light of its viscoelastic behaviour identified previously from cyclic and monotonic creep tensile tests. A procedure is proposed to identify the relaxation modulus from the cyclic indentation tests on linear viscoelastic materials using sharp indenter.

2. Finite element model and materials

The finite element model of a cyclic indentation experiment was created using Abaqus software (see Figure 1). The tests involved an axisymmetric rigid conical indenter with an opening angle of 70.3° or a spherical indenter with a radius of 10 µm penetrating a large deformable sample measuring 500 x 500 µm². The bottom surface of the sample is clamped and the horizontal displacements of the left edge (the axis of symmetry) are restrained. The impact of the boundary conditions, sample size, and mesh on the indentation curves had been investigated previously, and the optimal parameters were selected. The mesh in the square zone of 10 x 10 µm in the vicinity of the indenter was regular, with a size of 0.1 x 0.1 µm2, and the size of the elements progressively increased toward the of the sample. The contact was frictionless and the viscous procedure with geometric non-linearity was employed. The loading path was cyclic, with constant and equal loading and unloading times without any hold. The maximum and minimum forces were 10 mN and 0.5 mN, respectively. Several simulations of ten cycles were performed, with the total time of the test t_{test} presented in Table 1, while the time of each cycle was $t_{test}/10$. Each simulation included at least 4000 iterations.

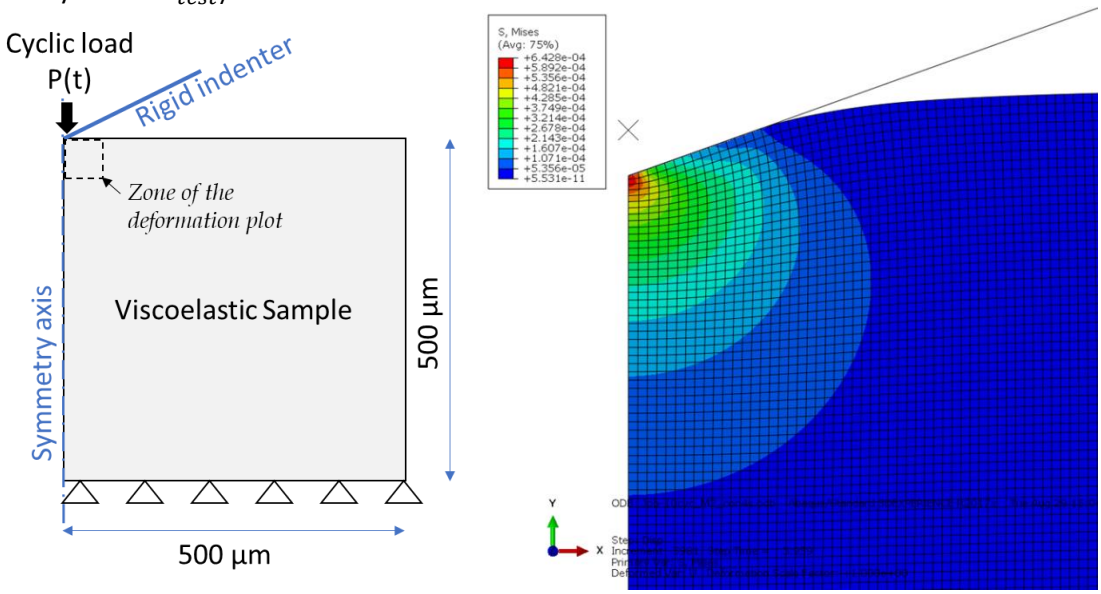

Figure 1. Schematic diagram of the finite element model and an example of deformation plot under maximum load.

t_{load}, s	2.10^{-5}	2.10^{-4}	2.10^{-3}	2.10^{-2}	2.10^{-1}	2.10^{0}	2.10^{1}	2.10^{2}	2.10^{3}
t_{test}, s	4.10^{-4}	4.10^{-3}	4.10^{-2}	4.10^{-1}	4.10^{0}	4.10^{1}	4.10^{2}	4.10^{3}	4.10^{4}
t_{load}/τ_{max}	5.10^{-6}	5.10^{-5}	5.10^{-4}	5.10^{-3}	5.10^{-2}	5.10^{-1}	5.10^{0}	5.10^{1}	5.10^{2}
t_{test}/τ_{max}	10^{-4}	10^{-3}	10^{-2}	10^{-1}	10^{0}	10^{1}	10^{2}	10^{3}	10^{4}

Table 1. Duration of the simulated tests and the ratio of the test time t_{test} to the maximum relaxation time τ_{max} of the materials MAT1 and MAT2.

The viscoelasticity was modeled with the Generalised Maxwell law available in Abaqus. The shear relaxation modulus $G(t)$ and bulk relaxation modulus $K(t)$ are defined as follows:

$$G(t) = G_0\left(1 - \sum_{i=1}^{N} g_i\left(1 - e^{-t/\tau_i}\right)\right) \quad \text{Eq. 1}$$

$$K(t) = K_0\left(1 - \sum_{i=1}^{N} k_i\left(1 - e^{-t/\tau_i}\right)\right) \quad \text{Eq. 2}$$

where G_0 and K_0 refer to the instantaneous shear and bulk moduli, and g_i and k_i are the weights of each viscoelastic branch with a relaxation time τ_i. The Poisson's ratio ν was chosen to be constant and equal to 0.4. Thus, the weights for shear and volumetric relaxation processes are equal ($g_i = k_i$), and the time-dependent relaxation modulus $E(t)$ can be described as follows:

$$E(t) = E_0\left(1 - \sum_{i=1}^{N} g_i\left(1 - e^{-t/\tau_i}\right)\right) \quad \text{Eq. 3}$$

Two materials with different relaxation spectra, as given in Table 2, were simulated. The instantaneous elastic modulus E_0 of both materials was equal to 4 GPa. The relaxation times were also similar between two materials, but the weights of each relaxation process differed. The maximum relaxation time, τ_{max}, was 4s. This simplified distribution is referred to as a double box and can be described by width and height of the two boxes instead of two parameters for each relaxation branch. The relative contribution of each box was inverted between the materials MAT1 and MAT2. In the former, the fast relaxation had a low weight in the overall relaxation process, and in the latter, its weight was significantly higher. That means that after 0.047s of the test, the modulus of MAT1 reaches $E(t = 0.047s) = 3.92\ GPa$, while the modulus of MAT2 reaches $E(t = 0.047s) = 2.4\ GPa$. The completely relaxed modulus is $E(t = \infty) = 1.36\ GPa$. The stabilization of the modulus at this value occurs after 20 s, or 5 τ_{max}, for MAT1, and 14s, or 3.5 τ_{max}, for MAT2.

These materials are not intended to represent a real polymer material. This distribution is greatly simplified compared to actual polymers, but it is more complex than simple analytical models that consider only one or two relaxation times studied in the literature, and it encompasses a wide range of relaxation times.

MAT1	$g_i = k_i$	0.01	0.01	0.08	0.08	0.08	0.08	0.08	0.08	0.08	0.08
MAT2	$g_i = k_i$	0.21	0.21	0.03	0.03	0.03	0.03	0.03	0.03	0.03	0.03
MAT1 & MAT2	τ_i, s	0.0078	0.0156	0.0313	0.0625	0.125	0.25	0.5	1	2	4
	τ_{max}/τ_i	512	256	128	64	32	16	8	4	2	1

Table 2. Distribution of the bulk k_i and shear g_i dimensionless weights and the relaxation times τ_i for materials MAT1 and MAT2.

3. Results and discussions

3.1. Force-displacement curves

The force-displacement curves resulting from the eight tests of 10 cycles, with t_{test}/τ_{max} varying between 10^{-3} and 10^{4} for MAT1 and 10^{-4} and 10^{3} for MAT2, are presented in Figure 3 and Figure 4, respectively. The loading time of each test varied between 2.10^{-4} s and 2.10^{3} s for MAT1, and 2.10^{-5}s and 2.10^{2} s for MAT2. These results show the evolution of the mechanical response, transitioning from purely elastic at very short test durations, through viscoelastic and hysteretic behavior in the intermediate range, to purely elastic at the longest test durations. Notably, all curves of 10 cycles are superposed for the first test for both materials. In the fastest test on MAT1, presented in Figure 2(a), the loading time is 5.10^{-5} times lower than the maximum relaxation time of materials τ_{max} and $2.56.10^{-2}$ times lower than the minimum relaxation time τ_{min} of the materials. At this loading time, MAT2 presents some evolution of the behaviour with cycles, see Figure 3(b), due to the higher weight of τ_{min}, 0.21 for MAT2 compared to 0.01 for MAT1, in the relaxation process. This effect is reversed in the tests with the longest time: MAT2 becomes elastic when the loading time is 50 times higher than τ_{max} (see Figure3(h)), while the behaviour of MAT1 remains slightly hysteretic at this loading rate (see Figure 2(g)). This can be explained by the weight of τ_{max} of 0.08 in MAT1 compared to its weight of 0.03 for MAT2.

In the first non-elastic tests on both materials presented in Figure 2(b, c, d) and Figure 3(b, c, d), the indentation cycles shift from left to right without establishing a closed loop. These are the tests with a cumulative test time that is lower than the time necessary for the material to stabilize its behavior. However, it is not straightforward to determine stabilization from the force-displacement curves only. The time of stabilisation will be estimated from the evolution of the area of the loop and discussed in Section 3.5. In contrast, in the second family of tests shown in Figure 2(e, f, g) and Figure 3(e, f, g), a stabilised loop is formed after some cycles or even from the first cycle, as in Figure 2(f, g) and Figure 3(g). The loop stabilizes from the beginning of the test with a loading time of 20s, or $5\tau_{max}$, for both MAT1 and MAT2. This indicates that the loading time is the characteristic time for this test and its ratio to the maximum relaxation time conditions the stabilization of the loop.

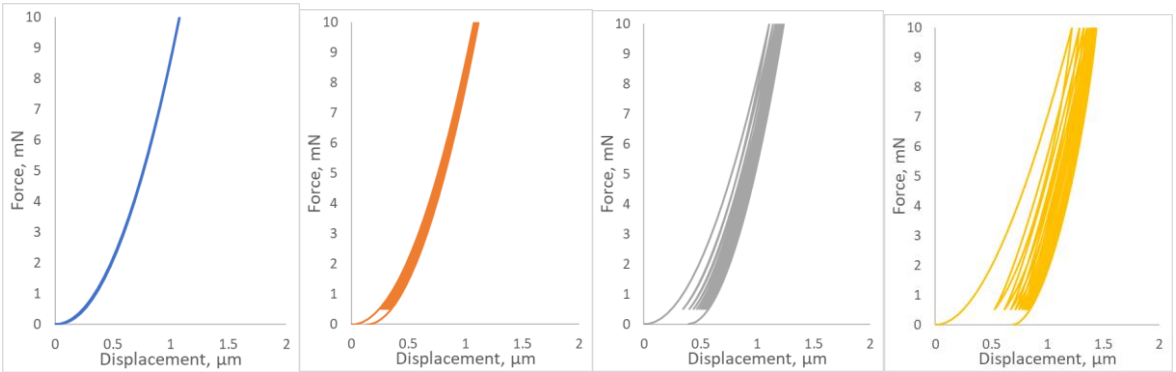

(a) (b) (c) (d)

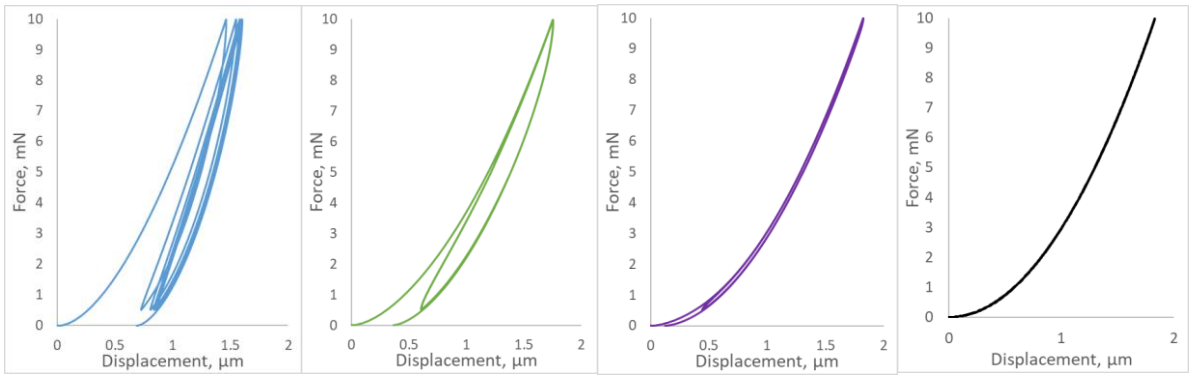

(e) (f) (g) (h)

Figure 2. Simulated indentation curves on MAT1 for the following ratios of t_{test}/τ_{max} : a) 0.001, b) 0.01, c) 0.1, d) 1, e) 10, f) 100, g) 1000, h) 10000.

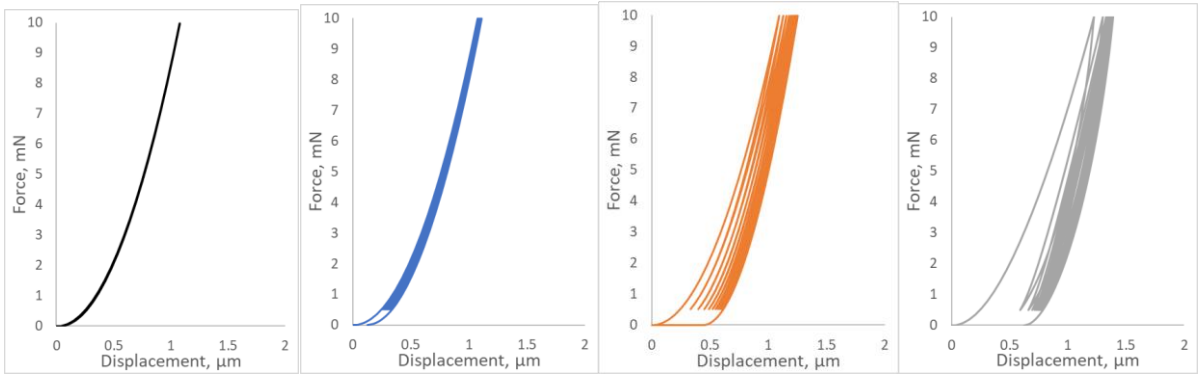

(a) (b) (c) (d)

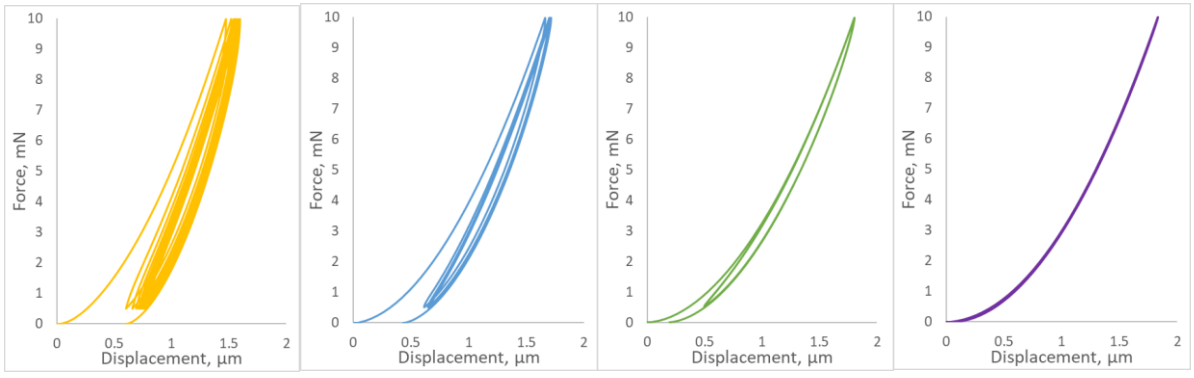

(e) (f) (g) (h)

Figure 3. Simulated indentation curves on MAT2 for the following ratios of t_{test}/τ_{max} : a) 0.0001, b) 0.001, c) 0.01, d) 0.1, e) 1, f) 10, g) 100, h) 1000

3.2. Analysis of viscoelastic indentation curves

In this section, the application of various analysis methods available in the literature for viscoelastic indentation curves will be examined. The primary aim is to obtain the relaxation elastic modulus as a function of time. The error due to the use of elastic or elastoplastic solutions will be evaluated, and available in the literature viscoelastic solutions will be discussed.

For a homogeneous, isotropic elastic material, the relationship between force and displacement depends on the shape of the indenter. For a cone with an opening angle θ, it is expressed as follows:

$$F_{con}(h) = \frac{2\tan\theta E_r}{\pi} h^2 \quad \text{Eq. 4}$$

This relation can be inverted to obtain the reduced modulus of contact E_r, which depends on the contact stiffness S and the projected contact area A_p for all indenter shapes as [26]

$$E_r = \frac{\sqrt{\pi} S}{2\beta\sqrt{A_p}} \quad \text{Eq. 5}$$

The contact stiffness at a given contact depth is obtained as the derivative of force with respect to displacement. The coefficient β has been extensively studied in the literature [27], and it has been found to vary between 1.0026 and 1.1 for a variety of experiments and FE simulations on elastic and elastoplastic materials. It is typically taken as 1.034 for the Berkovich indenter. If the indenter is rigid, the indentation elastic modulus EIT, which in theory is equal to Young's modulus E of the material, is obtained from the reduced modulus and Poisson's ratio as follows:

$$EIT = E_r(1 - \nu^2) \quad \text{Eq. 6}$$

For an ideal cone with an opening angle of 70.3°, the projected contact area is

$$A_{p\ con} = 24.5{h_c}^2 \quad \text{Eq. 7}$$

In the case of purely elastic behavior, the contact depth can be obtained from the total depth of indentation at any loading moment as follows:

$$h_{c\ EL\ con} = \frac{2}{\pi} h \quad \text{Eq. 8}$$

When the material is elastoplastic, the most commonly used method in instrumented indentation is that of Oliver and Pharr [5]. This method assumes that the material exhibits elastoplastic behavior under loading, while the unloading is elastic at least initially. In this case, the solution for elastic behavior, given by Eqs. 4-8, can be applied with the contact stiffness and the contact depth evaluated at the beginning of the unloading. In practice, to calculate the stiffness, the unloading curve is fitted with a power law equation

$$F = A(h - B)^m \quad \text{Eq. 9}$$

The contact depth is obtained from the following relationship:

$$h_{c\ O\&P} = h_{max} - \varepsilon F_{max}/S \quad \text{Eq. 10}$$

where ε is equal to 0.72 for elastic indentation with conical indenters. However, it is usually taken as 0.75, which corresponds to a spherical indenter, because of the evolution of the contact area during unloading.

Firstly, the application of contact depth estimation using the elastic (Eq.8) and elastoplastic (Eq. 10) solutions for the cyclic response of a viscoelastic material is examined by comparing them to the actual contact depth measured in FE simulations. To obtain the contact stiffness during loading and unloading, the data were fitted with Eq. 9 over 20-100% and 20-98% ranges, respectively. All the contact depth estimations, $h_{c\ O\&P\ load}$ and $h_{c\ O\&P\ unl}$ evaluated at the maximum load, $h_{c\ el}$ evaluated at each moment, and the measurement from FE simulation $h_{c\ FEM}$ are plotted in Figure 4 for one numerical test on Material 2 with $t_{test} = 0.4s$. To obtain $h_{c\ FEM}$, the contact pressure was analyzed along the path on the surface of the sample and the contact radius was set to the point where contact pressure drops to 0. The contact depth as a function of time is calculated as the difference between the displacement of the indenter and the vertical displacement of the point at the edge of contact.

It is evident from Figure 4 that the elastoplastic approach during unloading significantly overestimates the contact depth in all cycles. Using loading curves to evaluate contact stiffness at maximum load is

more accurate. The elastic formula provides a very accurate value of contact depth during the first loading and at the maximum load of each cycle. However, in the final stages of unloading, material retardation occurs as the indenter is removed, leading to an overestimation the contact depth by the elastic solution. When the indenter is completely removed, the elastic solution yields a contact depth value of 0.4 µm due to the residual impression.

Secondly, the quality of the fit for the loading and unloading curves was verified. It can be observed that several of the indentation curves presented in Figures 2 and 3 exhibit a "nose" effect during unloading. It is known that indenting a viscoelastic material can induce a negative stiffness at the beginning of the unloading phase. To avoid this, some authors [28] suggest evaluating the contact stiffness not at the maximum load but at a point after unloading has started. Unsurprisingly, despite the unloading being fitted up to 98 and not 100%, many of the unloading curves are poorly fitted with the Eq. 9. Moreover, the power law coefficient m, which is equal to 2 for cone and less than 2 for paraboloid, spherical and flat punch geometries, varies significantly for the simulated viscoelastic curves. Figure 5(a) presents the evolution of the power law coefficient m calculated from the loading and unloading of all cycles and tests as a function of the cumulative time t_{cumul} normalised by the maximum relaxation time τ_{max}.of the materials MAT1 and MAT2. The cumulative time of test t_{cumul} is defined as the mean time of each cycle, corresponding to the end of each loading phase where the elastic modulus is usually evaluated. The results in Figure 5(a) indicate that the power law coefficient is greater than 2 during unloading and lower than 2 during loading for all cases where viscoelastic hysteresis is present. However, a power law coefficient greater than 2 is theoretically impossible, as it would imply a concave indenter shape. The poor fit also affects the determination of the contact depth from unloading and contributes to its overestimation.

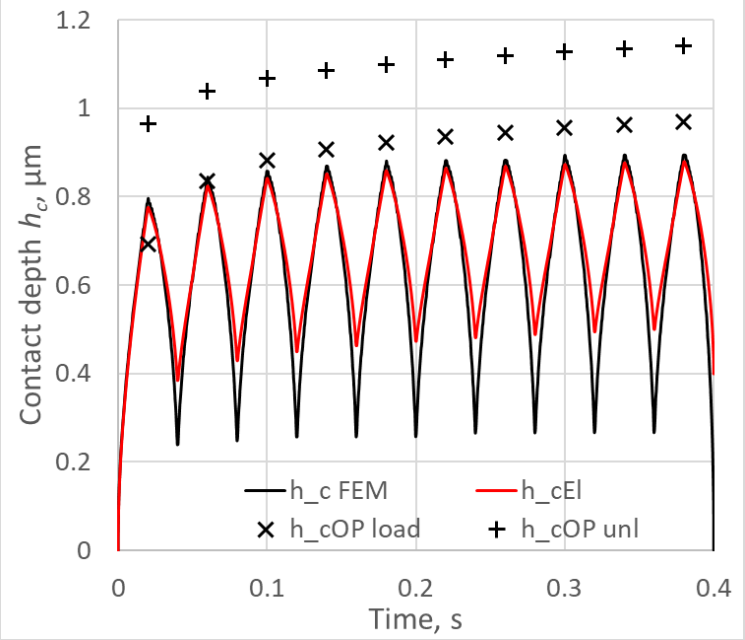

Figure 4. Evolution of contact depth with time for the 0.4s test with conical indenter.

Lastly, the elastic moduli at the end of each loading phase were evaluated using Eqs. 5 and 6 from two estimates of the contact depth, $h_{c\ O\&P\ unl}$ and $h_{c\ el}$, along with the loading S_{load} and unloading S_{unl} contact stiffnesses. Figure 5b presents the moduli of the first cycle from all tests as a function of time corresponding to the end of loading normalized by the maximum relaxation time of both materials. It appears that for all tests across the entire viscoelastic range of the materials, the moduli calculated from the unloading stiffness are higher than those obtained from the loading stiffness. The discrepancy is particularly pronounced in the intermediate time range, reaching a difference of 1.74

GPa for the cycle of $0.01\tau_{max}$ for Material 2 ($EIT_{O\&P\ unl} = 4.38\ GPa, EIT_{el\ load} = 2.64\ GPa$). In some cases, the elastic moduli evaluated from the unloading contact stiffness exceed the instantaneous elastic modulus of the materials $E_0 = 4\ GPa$, which invalidates the use of the unloading data. The overestimation of the elastic modulus by Oliver & Pharr method is related to both the overestimation of the contact depth and the incorrect stiffness with a high-degree power law.

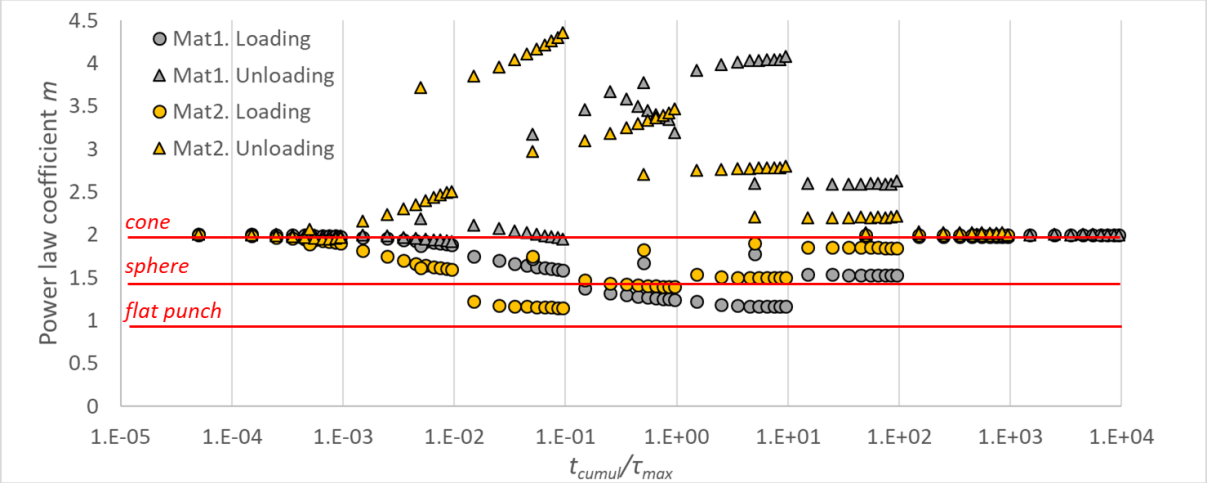

(a)

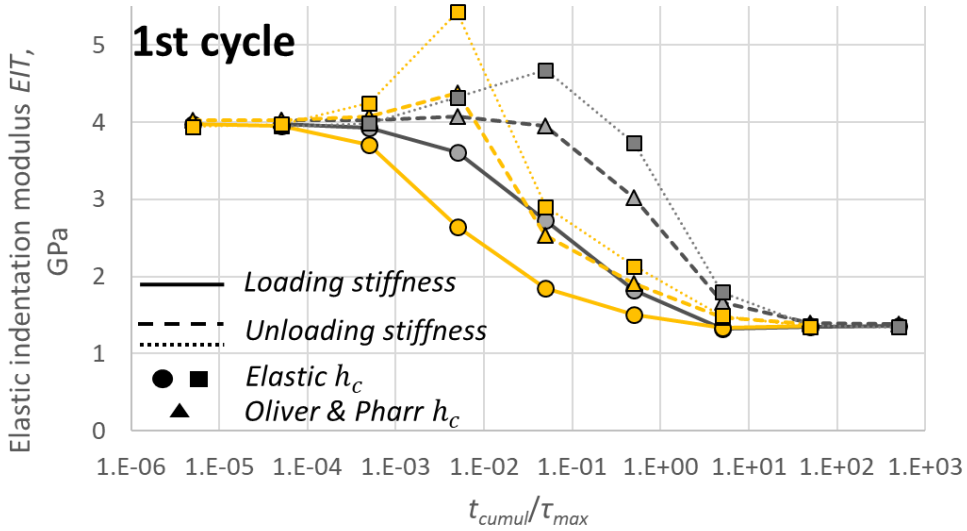

(b)

Figure 5. a). Power law coefficients m obtained from the fitting of loading and unloading curves in each cycle of each test b). Elastic indentation moduli of the first cycle of each test obtained using different combinations of contact stiffnesses and contact depths

3.3. Identification of the relaxation modulus from cyclic indentation tests

Based on the considerations presented in the previous section, the elastic indentation modulus for all cycles was calculated using the elastic contact depth corresponding to each maximum load and the contact stiffness obtained from the loading of each cycle. Initially, the β factor was set to 1. The values of the indentation elastic moduli for the slowest and fastest tests were compared with the instantaneous E_0 and relaxed E_∞ moduli of MAT1 and MAT2 to establish the value of the β coefficient. The values of $\beta = 1.029$ and $\beta = 1.035$ were obtained, respectively. These values are not significantly different from the 1.034 suggested in the literature for the Berkovich indenter, which was consequently applied to all the results.

The elastic indentation moduli obtained through elastic analysis from each loading are presented in Figure 6 as a function of cumulative time normalised by the maximal relaxation time of both materials, $\tau_{max} = 4s$. The relaxation moduli $E(t)$ of both materials defined by Eq.3 are also included in this figure for comparison. One can see that the indentation elastic modulus is stable for the first and last tests on the time scale, while it increases with cycles for the intermediate tests. The evolution of the elastic indentation modulus with cycles does not follow the relaxation modulus curve; however, the value of EIT of the first loading nearly coincides with the $E(t)$ curves for all tests. The small discrepancies that exist for some values can be attributed to the β value, which is slightly time-dependent, as explained in the previous paragraph. Thus, the evolution of the relaxation modulus with time can be derived from the first loading with different loading rates using elastic analysis.

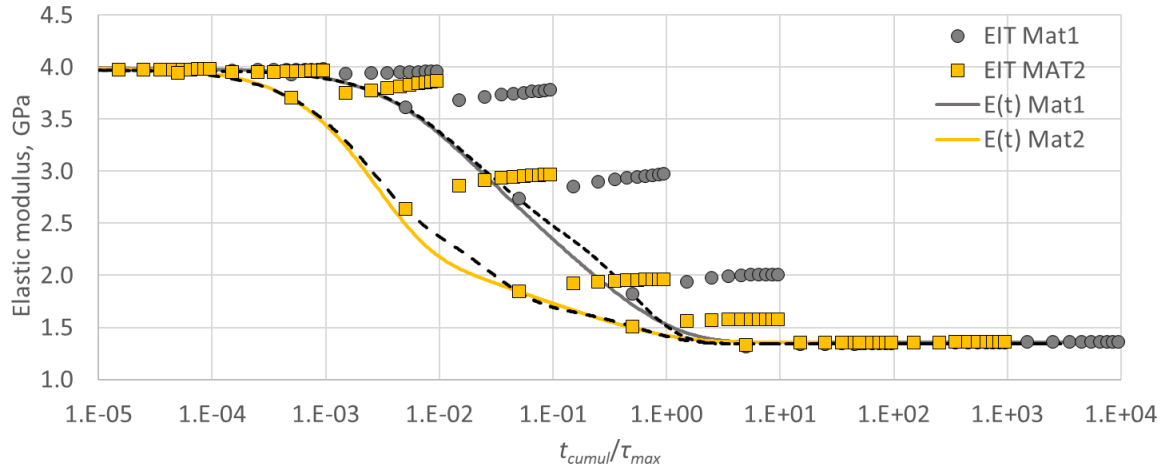

Figure 6. Instantaneous moduli calculated from the loading of all cycles in all the simulations for the two materials. Continuous lines represent the relaxation moduli of the two materials, while dashed lines indicate the fits using Generalised Maxwell law for the elastic indentation moduli from the first loading of each test. The parameters of these fits are presented in Table 3.

The indentation moduli obtained from the first loading, EIT_{1c}, of all tests were fitted using the Generalized Maxwell law, similar to Eq.3. Three relaxation processes were employed since only 8 points were available for fitting. The parameters of the fit are presented in **Erreur ! Source du renvoi introuvable.** and the resulting curves representing the evolution of relaxation moduli with time are shown in Figure 6 by dashed lines**Erreur ! Source du renvoi introuvable.**. It is evident that the transition region is not adequately described by only three viscoelastic branches. However, this can be improved if more experiments are conducted with loading times falling within this region. In the time range where the transition is no this rapid, the identified from the viscoelastic cyclic response curves are close to the relaxation moduli of both materials incorporated into the simulations.

	E_0, GPa	g_1	τ_1, s	g_2	τ_2, s	g_3	τ_3, s	R^2
MAT1 EIT_{1c}	3.976	0.133	0.032	0.191	0.138	0.338	1.937	0.9999
MAT2 EIT_{1c}	3.977	0.333	0.009	0.231	0.105	0.098	2.315	1

Table 3. Viscoelastic parameters identified from EIT_{1c} of 8 indentation tests with Eq.3.

These results indicate that it is not possible to identify relaxation times shorter than the loading time from cyclic loading. This is an important observation regarding experiments on real polymer materials, as the experimentally accessible loading rates cover only 2 or 3 decades on the logarithmic time scale, while many polymers relax over a larger time scale. If the loading rate is too short, nanoindentation equipment has difficulty following the change in loading direction, which can lead to a loading

overshoot in the resulting curves. Conversely, if the loading rate is too long, the experimental response becomes increasingly affected by thermal drift, which is challenging to correct for polymers. Usually, nanoindentation experiments on polymers are conducted in the transition range of the relaxation modulus, which, for the materials modeled with the Generalized Maxwell law, is $10^{-4} < t_{load}/\tau_{max} < 10$. Nevertheless, fitting the evolution of the elastic moduli obtained from the cyclic test with time using a viscoelastic law provides relaxation time constants that reflect the relaxation times of the tested material. Moreover, if stabilization of the force-displacement loop is observed, the maximum relaxation time of the material, τ_{max}, can be estimated from the time of stabilization.

3.4. Is it possible to obtain the instantaneous modulus from the unloading slope?

The finite element simulations conducted by Cheng and Cheng [20, 21] demonstrated that the unloading curves at different rates converged to a single curve, which provides the instantaneous elastic modulus E_0 from its stiffness when the unloading rate was "fast enough". In their simulations of a standard linear solid material, this unloading time was 0.01s, which corresponds to 0.01 of τ_1, the relaxation time of this material, when the loading time was 5s, or $5\tau_1$, in the displacement-controlled test, and 10s, or $10\tau_1$, in the load-controlled test. It is important to note that, in both cases, the entire viscoelastic relaxation was exhausted during loading ($t_{load} \geq 5\tau_{max}$). To match the elastic modulus obtained from the indentation with the one incorporated into the model, they introduced a correcting coefficient of $\alpha = 1.034$ for the contact depth and another coefficient $\beta = 1.06$ for the elastic modulus. Let us now examine the effect of the unloading rate on the contact stiffness over a wide range of t_{load}/τ_{max}. The aim is to verify whether there is a universal unloading rate that provides the instantaneous elastic modulus for any loading rate.

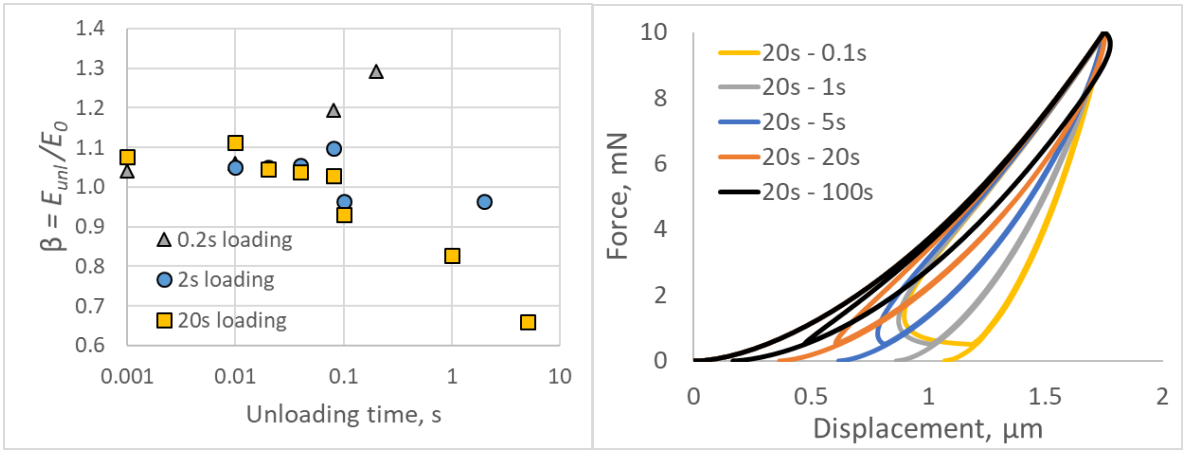

(a) (b)

Figure 7. (a) Normalized unloading elastic modulus of MAT1 for different loading and unloading times; (b) two cycles with a similar loading rate $t_{load} = 20s = 5\tau_{max}$ and different unloading rates ranging from 0.1 s to 100 s, simulated on MAT1.

The elastic moduli obtained from the initial stiffness of the unloading, S_{unl} , and the elastic contact depth $h_{c\,EL}$, normalized by the instantaneous elastic modulus E_0, are presented in Figure 7a. Different loading times in the range of 0.001 s to 5 s were tested following loading times of 0.2 s, 2 s and 20 s. All tests were performed in load control mode with a triangular loading-unloading trajectory and fall within the transition range of viscoelastic relaxation. It is not surprising that the values of E_{unl} depend on the unloading rate; however, the simulations reveal that it does not appear to be a universal "fast enough" unloading rate that would provide $E_{unl} = E_0$for all loading rates. The response is influenced by the loading rate and, in all tested cases, is either higher or lower than E_0. This indicates that the corrective β coefficient depends on both the loading and unloading rates.

It is interesting to note that the unloading rate does not affect the stabilization of the loops, as shown in Figure 7b. This figure presents two cycles with a loading time of $t_{load} = 20s = 5\tau_{max}$ and different unloading times ranging from 0.1 s ($0.025\tau_{max}$) to 100 s ($25\tau_{max}$). In all tests, the second cycle perfectly overlaps with the first one. While the elastic indentation modulus evaluated from the loading at maximum load is already relaxed and equal to E_∞, the unloading stiffness varies significantly depending on the unloading rate. The reloading curves all overlap at the upper part, and the maximum indentation depth h_{max} is the same in all tests and both cycles. It can be concluded that the unloading rate does not affect the elastic indentation modulus evaluated from the loading of the second cycle when stabilization occurrs from the first cycle.

3.5. Energy dissipation in cyclic indentation tests

The dissipated energy in each cycle is usually evaluated by considering the part of irreversible work W_{irr} in the total work W_{load} of indentation [19, 25]. This energy ratio, denoted as η, is calculated as follows:

$$\eta = \frac{W_{load} - W_{unl}}{W_{load}} \times 100\% = \frac{W_{irr}}{W_{load}} \times 100\% \qquad \text{Eq. 11}$$

To examine the viscoelastic dissipation and the stabilization of the behaviour with time, the energy ratio η is plotted for the entire range of tests with both materials in Figure 8. It can now be established that the dissipation is actually close to zero in the first tests with $t_{load}/\tau_{max} = 5.10^{-5}$, which corresponds to $t_{load}/\tau_{min} < 0.0256$ for MAT1 ($\eta = 0.25\%$) and $t_{load}/\tau_{max} = 5.10^{-6}$ for MAT2 ($\eta = 0.16\%$). The dissipation is also almost negligible in the last test of $t_{load}/\tau_{max} = 500$ of MAT1 ($\eta = 0.45\%$). Stabilization occurs from the beginning when the energy ratio does not evolve during cyclic tests. The previous sections demonstrated that the loading time is responsible for the stabilization of the relaxation modulus. Thus, it is interesting to examine the ratio of the loading time to the characteristic relaxation times of the materials that provide stabilization. This is the case for the tests with both materials when $t_{load}/\tau_{max} > 5$. When the loading time is higher than $0.0256\tau_{min}$ and lower than $5\tau_{max}$, the energy ratio decreases during the cyclic test. This decrease follows the exponential relaxation law of the material and can be fitted with one or more relaxation times. The results also show that the stabilization of the loop occurs in the tests with $t_{load}/\tau_{max} = 0.5$ after several cycles when the cumulative test time is higher than $3.5\tau_{max}$ for MAT1 and MAT2. This indicates that the evolution of the energy ratio with cycles describes the long relaxation behavior of the material. Thus, it might be interesting to apply many cycles to obtain the stabilization of the loop and estimate the maximum relaxation time of the material. However, the time scale of this process is logarithmic, and the stabilization may not be attainable in a reasonable time frame for an experiment.

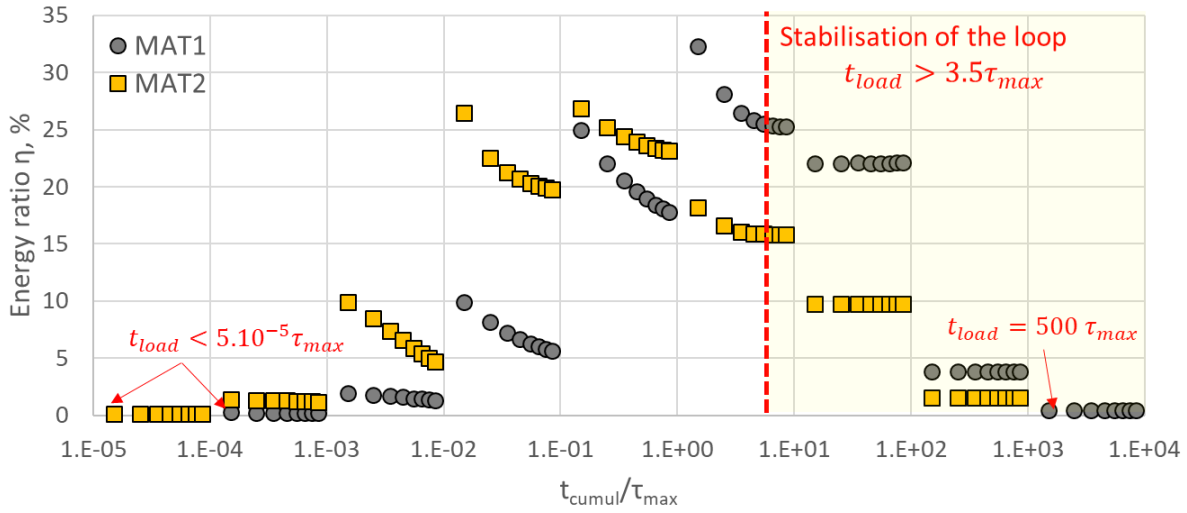

Figure 8. Energy ratio η of all simulations for all cycles but the first and the last ones.

When $t_{load}/\tau_{max} = 5$, as shown in Figure 7b, and the loop is stabilized from the beginning regardless of the unloading rate, the energy ratio calculated from the second cycle decreases from 51.2% for the fastest unloading (0.1s) to 16% for the slowest one tested (100s). The simulations do not indicate whether a completely anhysteretic behavior can be achieved when the unloading time is very long. However, a significant "nose" is visible during the unloading at 100s.

3.6. Cyclic versus monotonic indentation creep

Viscoelasticity is often characterized by indentation creep tests, where the load is kept constant for a long time after loading, and the indentation depth continues to evolve due to the retardation of the viscoelastic response of the material. The evolution of the depth during the holding period is fitted with viscoelastic rheological models to estimate the time constants of the tested material [6, 9, 12]. However, since the loading is not instantaneous, the creep behavior is affected by the loading time, similarly to the tension creep test. Thus, it is difficult to relate the time constants obtained from the fitted indentation creep curve to the time constants of the tested material. Another, and even more significant, problem with this test is that the constant indentation load does not imply constant stress. The time constants identified from the indentation creep may not be comparable to those measured under uniaxial tensile loading.

The indentation creep test was simulated on MAT1 and MAT2 with a loading time of $0.00002\ s$ ($0.0025\tau_{min}$) and a holding time of 400 s ($100\tau_{max}$) at the maximum load of 10 mN, as in the cyclic tests. The finite element simulations reveal that the compressive stress and strain in the area under the indenter relax with time. At the same time, they increase in the area around the indenter due to its sinking under constant load and the increase in the tested volume. This behavior is well-documented in the literature for viscoelastic materials [15, 16].

It is interesting to note that the elastic modulus obtained by the Oliver and Pharr method from the unloading in $0.00002\ s$ following 400s of creep on MAT2 is equal to 3.05 GPa, which is far from $E_0 = 4\ GPa$. This confirms that a very long holding of the constant load, combined with a very fast unloading, does not necessarily provide the instantaneous modulus from the unloading.

The relationships between cyclic creep and monotonic creep under tension have been studied in polymers both experimentally and numerically [29, 30]. This relationship is of particular interest for models when ratcheting behavior conditions damage and the fatigue life of polymers. It will now be examined from the perspective of indentation of a viscoelastic material.

The indentation cyclic creep is defined as the evolution of the indentation depth h_{max} at maximum load F_{max} of each cycle with time. The comparison between the cyclic creep and the monotonic indentation creep on MAT1 and MAT2 is shown in Figure 9. One can note that the evolution of indentation depth in the monotonic load test qualitatively resembles the curves of the relaxation moduli of both materials (see Figure 6). It is constant during the initial moments after loading and becomes constant again after around $7\tau_{max}$. Once the relaxation has finished, the indentation depth becomes the same, namely 1.84 µm, for both materials. The indentation depth at maximum load of each cycle h_{max} in all tests follows the same tendency and superposes on the monotonic creep curves in the shortest and longest tests. For the tests in the transition region, the cyclic creep is lower than the monotonic creep. This is due to the longer loading in cyclic test for the first cycle and the contribution of the unloading to the other cycles. However, the tendency of evolution of h_{max} with cycles in each test resembles the evolution of the elastic modulus shown in Figure 6, i.e., it increases with time. The stabilization of the loops, observed in the energy ratio previously, also impacts h_{max}. If the loop is stabilized, the cyclic creep will never reach the indentation creep under constant load.

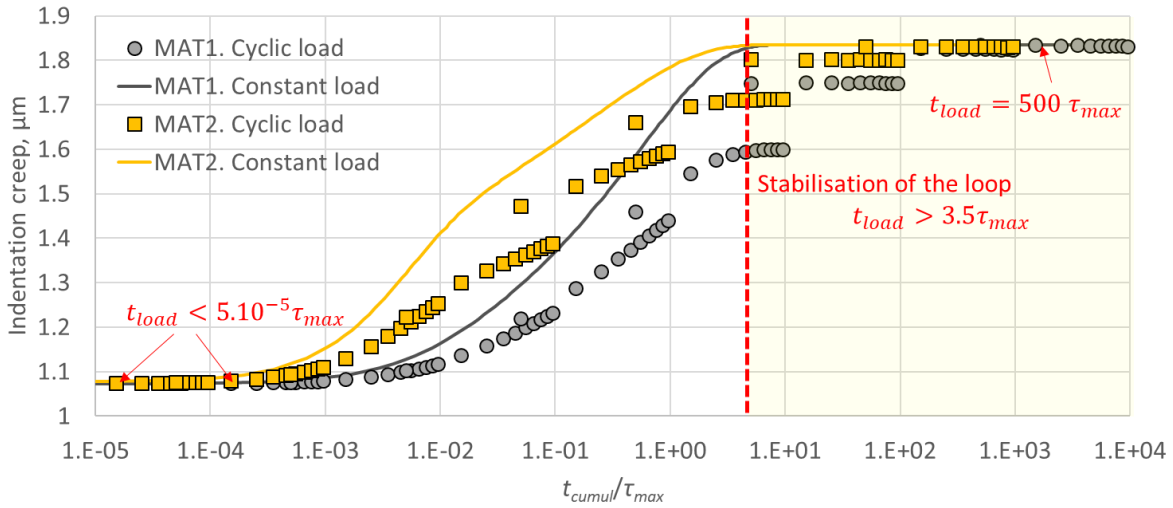

Figure 9. Cyclic creep (h_{max} of each cycle) and monotonic creep for two materials.

The linearity of the constitutive law provides a simple relation between monotonic and cyclic creep. Looking at the trends presented in Figure 9, one can note that the evolution of the maximum indentation depth of the first loading, h_{max1}, with time follows the same tendency as the monotonic creep but is constantly shifted on the time scale to longer times. A near-perfect superposition is obtained with a ratio of 2.5, such that $h(t_{cr}) = h_{max1}(t_{load}/2.5)$, as demonstrated in Figure 10. In these relations, t_{cr} is the time of the monotonic creep test elapsed from the beginning of the creep, which started $2.10^{-5}\ s$ after the beginning of the test and $h(t_{cr})$ is the temporal evolution of the indentation depth under constant load.

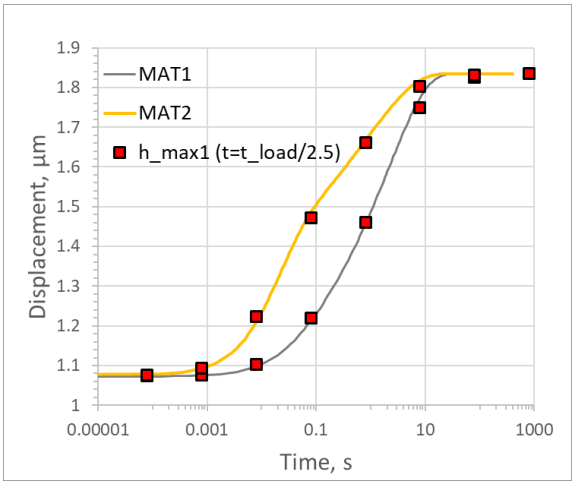

Figure 10. Superposition of the monotonic creep and the shifted indentation depth of the first cycle.

3.7. Cyclic indentation with spherical indenter

When one seeks to characterize the viscoelastic behavior of a polymer material, it is a good idea to use a spherical indenter since the stress concentration under the tip is less pronounced and plastic behavior can be limited or completely avoided. In the case of a spherical indenter, the contact mechanics equations of the elastic solution presented in Section 3.2 apply as well, with only a difference in the contact depth and the projected contact area of the indenter. The former is defined from the maximal depth of indentation as

$$h_{c\,EL\,sph} = \frac{h_{max}}{2} \qquad \text{Eq. 12}$$

while the latter is defined as follows:

$$A_{p\,shp} = \pi(2Rh_c - h_c^2) \qquad \text{Eq. 13}$$

where R is the radius of the indenter. The elastic indentation modulus can then be calculated using Eq. 5.

The cyclic indentation behavior of MAT1 under a spherical tip with the radius of 10 µm was simulated using the same finite element model and loading protocol as for the conical indentation. The resulting force-displacement curves were similar to those of the conical indenter, but the indentation depth was generally lower. First, the elastic contact depth defined by Eq. 12 was compared with the actual contact depth measured in the FE model. The result, presented in Figure 11(a), shows that the contact depth of the viscoelastic material in contact with a sphere is again better represented by the elastic contact formula, Eq. 13, than by the Oliver & Pharr method. The indentation elastic moduli, energy ratio and cyclic creep are compared between the results of the conical and spherical indentations in Figure 11(b-d). The same analysis method used for the conical indenter, with $\beta = 1.034$ and Eqs. 12 and 13 for the contact depth and contact area, was applied to obtain the elastic modulus from the spherical indentation. It is clear that the elastic moduli and energy ratio are nearly the same for both conical and spherical indentations, and all the conclusions drawn for the indentation with cone also hold for the sphere. Since the contact depth is lower with the sphere, there is a difference in cyclic indentation creep between the two indenters. However, as shown in Figure 11(d), the maximum indentation depth h_{max} of all the tests and cycles is simply shifted to a lower depth by a constant value.

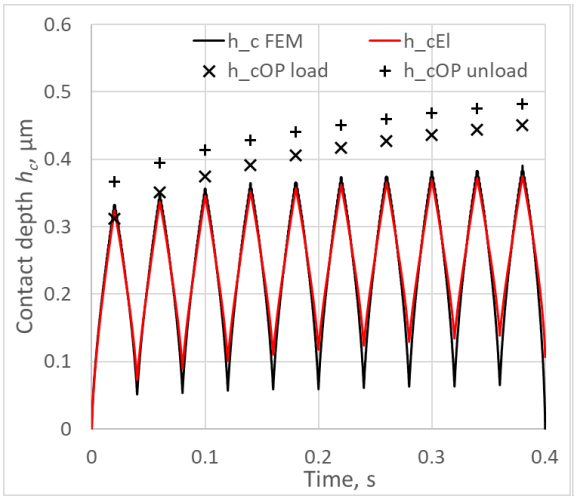

(a)

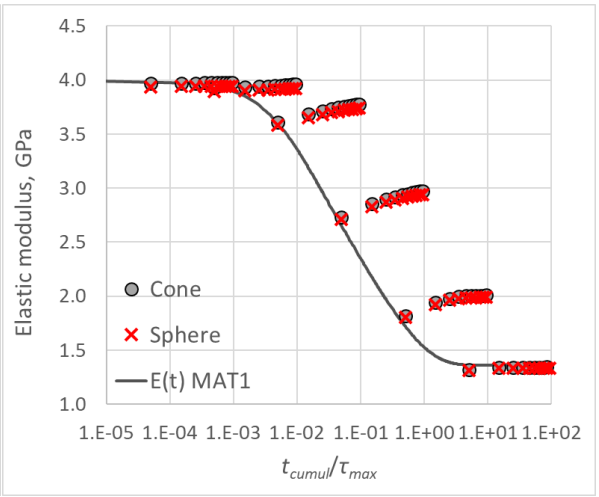

(b)

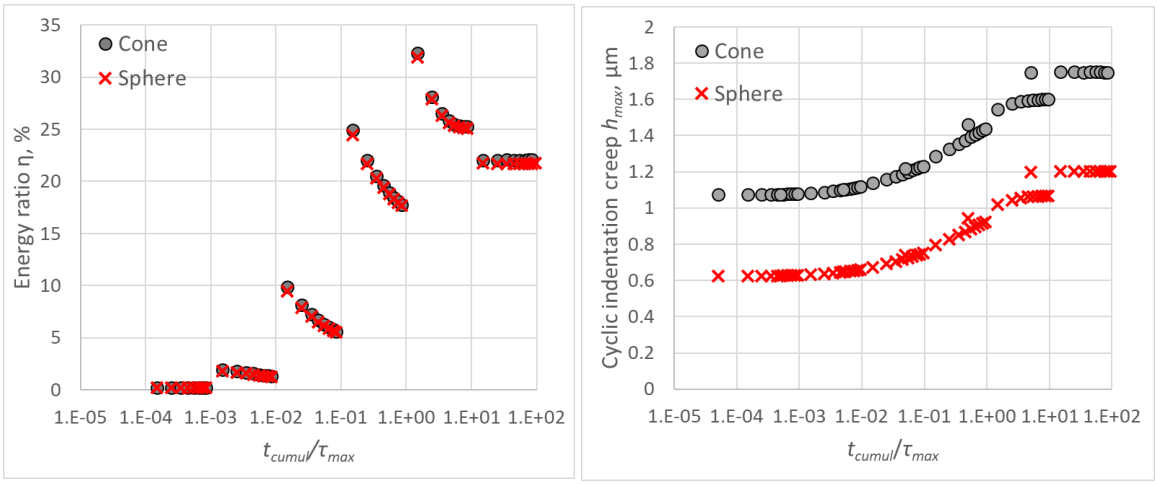

(c) (d)

Figure 11. Contact depth with spherical indenter (a) and comparison of elastic modulus (b), energy ratio (c) and cyclic creep (d) between the results obtained with conical and spherical tips on MAT1.

4. Comparison with experimental results of cyclic nanoindentation of a polymer using a Vickers tip

To evaluate the relevance of cyclic indentation loading to study viscoelasticity of polymeric materials and to compare the simulated response with experimental results, a previously published dataset [25] was analyzed using the proposed method. In this study, the mechanical response of high-density polyethylene (HDPE) to cyclic indentation loading was obtained using a pyramidal Vickers indenter. The loading trajectory was triangular, consistent with the current simulation, with loading times of $0.5\ s$, $4.8\ s$ and $47.5\ s$, and maximum and minimum loads of 10 mN and 0.5 mN, respectively. The number of applied cycles varied from 60 for the longest loading time to 1200 for the shortest. The force-displacement curves for characteristic cycles at the three loading times are presented in Figure 12.

The parameters identified for the same HDPE material in cyclic uniaxial tensile stress-controlled tests [31] were used as references for this nanoindentation study. In this work, the behavior of the polymer was found to be non-linear viscoelastic and was described by a small strain isothermal Maxwell-like constitutive model with a non-linear relation between stress and strain. The relaxation times varied from 0.8 s to 80000 s, and the weights were distributed between two plateaus (as in MAT2 in this study) with a smooth transition between 150 s and 1500 s. The instantaneous and relaxed elastic shear and bulk moduli were found to be $E_0 = 1.04\ GPa$ and $E_\infty = 0.83\ GPa$, respectively. The evolution of loops with frequency and the ratchetting behavior were qualitatively similar between tensile and indentation tests on the same material.

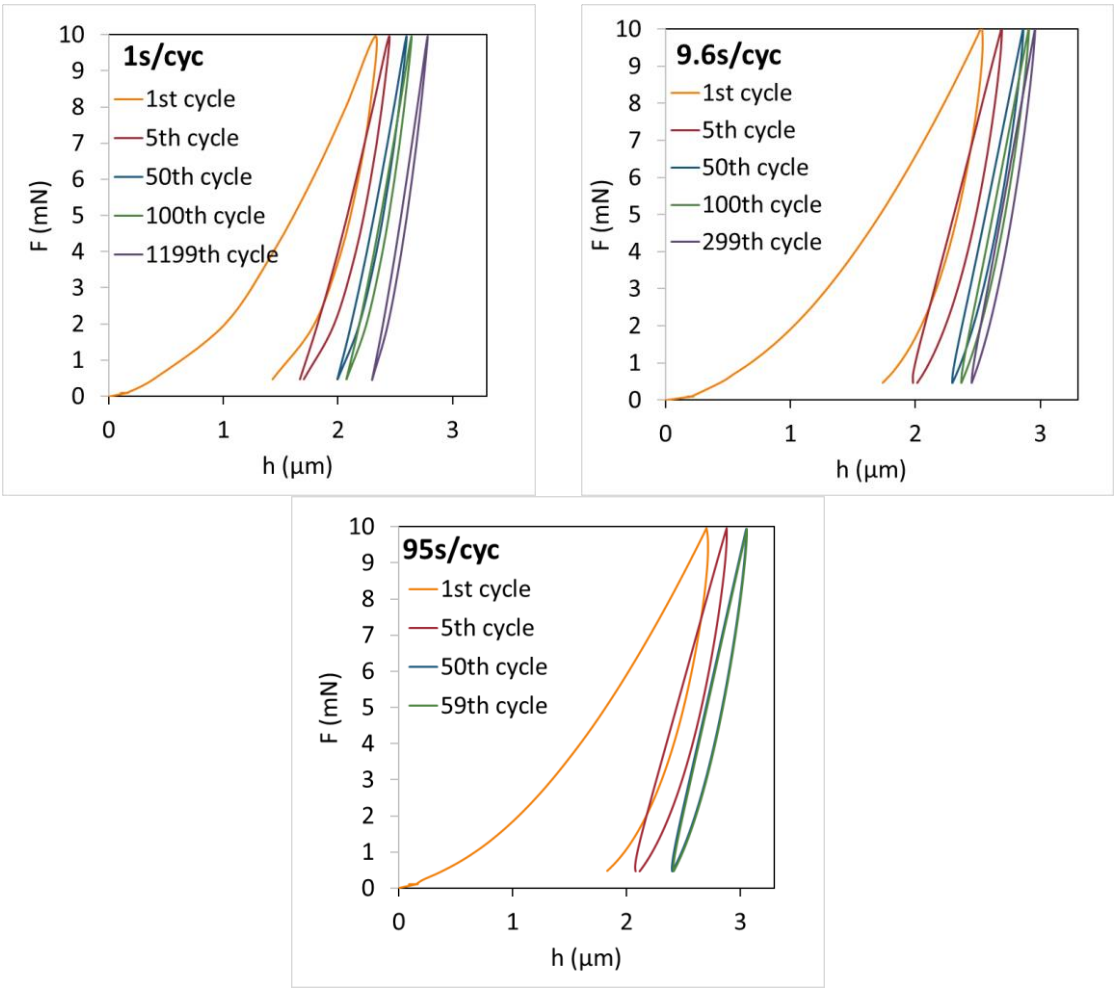

Figure 12. Experimental force-displacement response measured on High-Density Polyethylene (HDPE) for different durations of a cycle, with similar loading and unloading times of (a) $0.5\ s$, (b) $4.8\ s$ and (c) $47.5\ s$.

Figure 13 presents the results of the analysis conducted according to the method presented in this paper, applied to the experimental cyclic indentation data. There are six indentation tests for each condition, which are averaged, and the standard deviation is represented as the error bar. The evolutions of $h_{c\ O\&P}$ and $h_{c\ el}$ with time are shown in Figure 13(a). These data closely resemble those observed in the FE simulations using the Generalised Maxwell law (see Figure 4). Figure 13(b) presents the elastic moduli obtained from the elastic contact depth $h_{c\ el}$ and the contact stiffness at the end of each loading phase, with Poisson's ratio set at 0.4. Note that the elastic indentation moduli calculated using the contact depth $h_{c\ O\&P}$, obtained from the loading and unloading contact stiffnesses by the Oliver & Pharr method, were presented previously [25]. The energy ratio and cyclic creep evolutions with time are shown in Figures 13(c) and (d), respectively. The results from the three tests are qualitatively similar, and none of the parameters stabilize within the tested time range. The error bars from the six tests are small and are only visible in Figure 13(d), indicating that the results are not significantly affected by thermal drift.

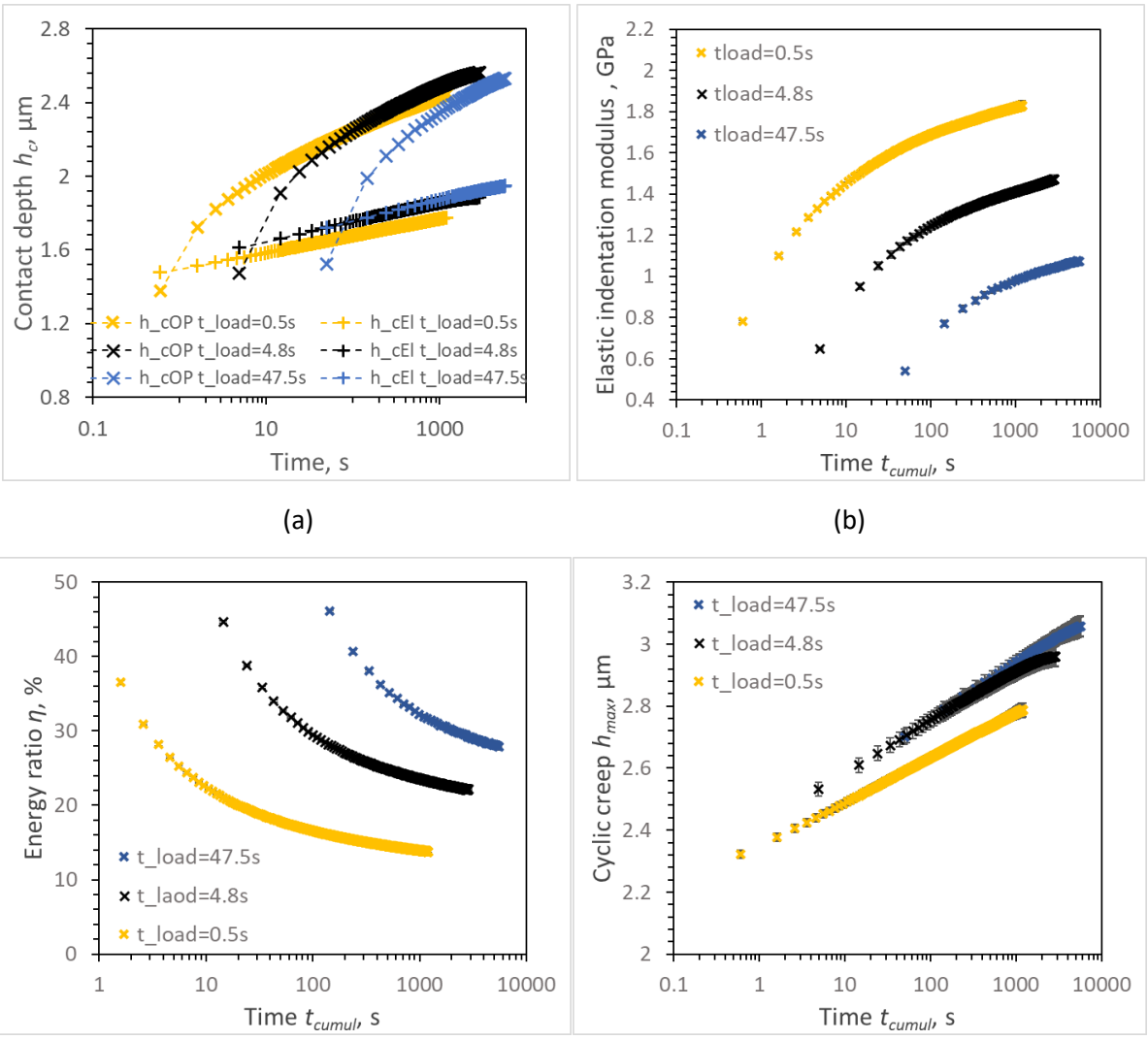

Figure 13. Experimental values of contact depth (a), elastic indentation modulus (b), energy ratio (c) and cyclic creep (d) measured with a Vickers indenter on the High-Density Polyethylene (HDPE) polymer.

Comparing the experimental nanoindentation results with those of the FE simulations presented in this study, it can be noted that they are qualitatively similar to the numerical results within the time range at the beginning of the transition $0.001 < t_{cumul}/\tau_{max} < 0.1$. The absence of the stabilization in the tested time range is consistent with the maximum relaxation time identified in the tensile tests, $\tau_{max} = 80000\ s$. None of the indentation tests lasted this long; therefore, it is natural that the entire spectrum of the viscoelastic modulus cannot be identified from these indentation tests. However, the experimental data can be used to attempt to identify the viscoelastic relaxation modulus at three loading times.

Since a pyramidal indenter was used in these tests, the formation of a plastic core around the tip is very likely. The indentation results are thus affected by this plasticity and cannot be analyzed within an elastic framework. To address this issue, we hypothesize that only the first loading is affected by plasticity. To obtain the relaxation modulus using the elastic equation (Eq.5), it is necessary to calculate the contact stiffness and the projected contact area at the time corresponding to the end of the first loading. The plastic depth can be estimated from the residual indentation depth after the

viscoelastic strain has recovered. In one of the experiments on the HDPE material published in [25], holding period at a small force of 0.1 N was applied for 3000 s after cyclic loading for 3000 s, during which the residual depth was measured at approximately 1.5 µm. Considering that the recovery was not complete and was measured under a small load, we will assume that the actual plastic depth, h_p, is 1 µm. In this case, the projected contact area can be obtained using the corrected viscoelastic indentation depth h_{cVE}, given by the following equation:

$$h_{cVE} = \frac{2}{\pi}\left(h_{max} - h_p\right) \qquad \text{Eq. 14}$$

To obtain the contact stiffness corresponding to the end of loading of the first cycle, it is possible to use the loading contact stiffnesses from the subsequent cycles and extrapolate them to the time t_{load}.

The loading stiffnesses S_{load} of the cycles from the second to the fifth were fitted using the following equation, which is similar to the Generalized Maxwell law with one viscoelastic branch:

$$S_{load}(\mathrm{t}) = a_E + \mathrm{b_E}\left(1 - \exp\left(-\frac{\mathrm{t}}{c_E}\right)\right) \qquad \text{Eq. 15}$$

The quality of fit of the stiffness curves with this equation was good, and the R^2 coefficients were higher than 0.996 in each case. The coefficients of fit, a_E, b_E and c_E, are given in Table 4, along with the relaxation moduli calculated directly from the first loading, EIT_{VE}, and the relaxation moduli, EIT_{VEP}, obtained from the extrapolated stiffness S_{load} and the corrected viscoelastic depth h_{cVE}.

As expected, the elastic moduli obtained directly from the first loading, EIT_{VE}, are lower than those extrapolated from the fitting, EIT_{VEP}. The short-time modulus ($t_{load} = 0.5\ s$) is higher than the instantaneous tensile modulus of 1.04 GPa when the viscoelastic-plastic hypothesis is applied, but lower when considering pure viscoelastic behavior. The moduli obtained from the longest tests ($t_{load} = 47.5\ s$) can be compared with the relaxed tensile modulus of 0.83 GPa. This value is close to that obtained with the viscoelastic-plastic behavior but is higher than that estimated with pure viscoelastic behaviour. The difference may be attributed to the non-linearity of the viscoelastic behavior or to the viscoplasticity of the plastic core, which are not considered in the indentation law.

t_{load}, s	a_E, GPa	b_E	c_E, s	EIT_{VEP}, GPa	EIT_{VE}, GPa
0.500	1,03	0,85	1,96	1,22	0.781
4.800	0,87	0,68	17,29	1,04	0.649
47.500	0,73	0,48	170,72	0,84	0.541

Table 4. Fitted values for the experimental cyclic indentation data on the High-Density Polyethylene (HDPE).

5. Conclusions

This paper presents a study of the mechanical response to cyclic indentation loading of viscoelastic materials described by the Generalized Maxwell law. The results are similar for conical and spherical indenters, assuming a linear viscoelastic response in both cases. Finite element simulations across the entire range of relaxation of two artificially created materials revealed the evolution of the cyclic response, transitioning from purely elastic behavior at very short time, when $t_{load}/\tau_{min} < 0.00256$, through hysteretic behavior with ratcheting and hysteretic behavior with a stabilized loop, to purely elastic behavior again at long times, when $t_{load}/\tau_{max} > 500$. The stabilization of the loop occurs at $t = 3.5\tau_{max}$ from the beginning of the test, independent of t_{load}. The analysis of the force-displacement curves revealed that it is possible to identify the relaxation modulus $E(t)$ of the viscoelastic material by using the equation of elastic contact depth with the contact stiffness computed from the first loading. This provides the values of $E(t)$ at $t = t_{load}$ from each indentation test. By varying the loading time of the test, it is theoretically possible to identify the relaxation modulus across the complete time range.

The effect of unloading rate across the range of loading rates on the elastic modulus evaluated from the beginning of unloading was investigated. The results revealed the absence of a converged unloading curve, which would provide the instantaneous elastic modulus, as suggested in the literature [20, 21]. In contrast, the unloading elastic modulus was either higher or lower than the instantaneous modulus for all tested unloading and loading rates.

A relation between indentation creep, defined as the evolution of the indentation depth with time under constant load, and cyclic indentation creep, defined as the evolution of maximum indentation depth, h_{max}, with time, was also studied. The evolution of h_{max} in cyclic tests follows the same viscoelastic trend as the elastic indentation modulus. Simple linear time shifts were observed between the indentation depth under monotonic creep tests and the indentation depth after the first loading at different rates.

Finally, the results of the numerical simulations were compared with the experimental results of the cyclic indentation tests on the high-density polyethylene (HDPE) polymer. The trends in the evolution of contact depth, elastic moduli, energy ratio and maximum indentation depth are very similar to the transitional behavior of the simulated viscoelastic materials described by the Generalized Maxwell law. To account for the impact of plasticity developed around the tip of the sharp indenter, the relaxation modulus was identified by fitting the loading contact stiffnesses of subsequent cycles and extrapolating to $t = t_{load}$. The contact depth was corrected by a constant plastic depth value estimated from the recovery after cyclic loading. The relaxation moduli of the HDPE at three different loading times were identified, falling within the range between the instantaneous and relaxed modulus identified on this material from previous cyclic tensile tests. It should be noted that the behavior of the polymer was likely affected by non-linear viscoelasticity and possibly viscoplasticity, which complicates the comparison with the Generalized Maxwell law.

Acknowledgments

Pprime Institute gratefully acknowledges “Contrat de Plan Etat - Région Nouvelle-Aquitaine” (CPER) as well as the “Fonds Européen de Développement Régional (FEDER)” for their financial support to the reported work.

References

1. R. F. Gibson, A review of recent research on nanoindentation of polymer composites and their constituents, Composites Science and Technology, Volume 105, 2014,Pages 51-65, https://doi.org/10.1016/j.compscitech.2014.09.016 .
2. M. Hardiman, T.J. Vaughan, C.T. McCarthy, A review of key developments and pertinent issues in nanoindentation testing of fibre reinforced plastic microstructures,Composite Structures, Volume 180, 2017, Pages 782-798, https://doi.org/10.1016/j.compstruct.2017.08.004 .
3. Y. Gaillard, F. Amiot, Grid nano-indentation as full-field measurements, Composites Part A: Applied Science and Manufacturing, Volume 132, 2020, 105807, https://doi.org/10.1016/j.compositesa.2020.105807 .
4. M. Pecora, O. Smerdova, M. Gigliotti, Gradients of cyclic indentation mechanical properties in PR520 epoxy and its 3D carbon fiber composite induced by aging at 150 °C, Polymer Degradation and Stability, Volume 193, 2021, 109720, https://doi.org/10.1016/j.polymdegradstab.2021.109720 .
5. W. Oliver and G. Pharr, An improved technique for determining hardness and elastic modulus using load and displacement sensing indentation experiments. J. Mater. Res. 7, 1564 (1992).
6. M. Oyen and R. Cook: Load–displacement behavior during sharp indentation of viscous–elastic–plastic materials. J. Mater. Res. 18, 139 (2003).
7. M.C. Barick, Y. Gaillard, A. Lejeune, F. Amiot, F. Richard, On the uniqueness of intrinsic viscoelastic properties of materials extracted from nanoindentation using FEMU, International Journal of Solids and Structures, Volume 202, 2020, Pages 929-946, https://doi.org/10.1016/j.ijsolstr.2020.03.015 .

8. V. Le Saux, Y. Marco, G. Bles, S. Calloch, S. Moyne, S. Plessis, P. Charrier, Identification of constitutive model for rubber elasticity from micro-indentation tests on natural rubber and validation by macroscopic tests, Mechanics of Materials, Volume 43, Issue 12, 2011, Pages 775-786, https://doi.org/10.1016/j.mechmat.2011.08.015.
9. B. Beake. Modelling indentation creep of polymers: a phenomenological approach. Journal of Physics D: Applied Physics, Volume 39, Number 20, 2006, 4478-4485, doi:10.1088/0022-3727/39/20/027
10. T. Chudoba and F. Richter: Investigation of creep behavior under load during indentation experiments and its influence on hardness and modulus results. Surf. Coat. Technol. 148, 191 (2001).
11. G. Feng and A. Ngan: Effects of creep and thermal drift on modulus measurement using depth-sensing indentation. J. Mater. Res. 17, 660 (2002).
12. M. Beyaoui, P.-E. Mazeran, M.-F. Arvieu, M. Bigerelle, M. Guigon Analysis of nanoindentation curves in the case of bulk amorphous polymers Int J Mater Res, 100 (2009), pp. 943-949, 10.3139/146.110137
13. E.G. Herbert, W.C. Oliver, and G.M. Pharr: Nanoindentation and the dynamic characterization of viscoelastic solids. J. Phys. D: Appl. Phys. 41, 1 (2008).
14. C.C. White, M.R. Vanlandingham, P.L. Drzal, N-K. Chang, and S-H. Chang: Viscoelastic characterization of polymers using instrumented indentation. II. Dynamic testing. J. Polym. Sci., Part B: Polym. Phys. 43, 1812 (2005).
15. Lee, E. H., and Radok, J. R. M. (September 1, 1960). "The Contact Problem for Viscoelastic Bodies." ASME. J. Appl. Mech. September 1960; 27(3): 438–444. https://doi.org/10.1115/1.3644020
16. T. C. T. Ting, The Contact Stresses Between a Rigid Indenter and a Viscoelastic Half-Space, *J. Appl. Mech*. Dec 1966, 33(4): 845-854 (10 pages) https://doi.org/10.1115/1.3625192
17. L. Cheng, X. Xia, L.E. Scriven, W.W. Gerberich, Spherical-tip indentation of viscoelastic material, Mechanics of Materials, Volume 37, Issue 1, 2005, Pages 213-226, https://doi.org/10.1016/j.mechmat.2004.03.002 .
18. M. Vandamme and F-J. Ulm: Viscoelastic solutions for conical indentation. Int. J. Solids Struct. 43, 3142 (2006).
19. Y.-T. Cheng and C.-M. Cheng, "Scaling, dimensional analysis, and indentation measurements," *Materials Science and Engineering: R: Reports,* vol. 44, pp. 91-149, 2004.
20. Cheng, YT., Cheng, CM. Relationships between initial unloading slope, contact depth, and mechanical properties for conical indentation in linear viscoelastic solids. Journal of Materials Research 20, 1046–1053 (2005). https://doi.org/10.1557/JMR.2005.0141
21. Cheng, YT., Cheng, CM. General relationship between contact stiffness, contact depth, and mechanical properties for indentation in linear viscoelastic solids using axisymmetric indenters of arbitrary profiles *Appl. Phys. Lett.* 87, 111914 (2005) https://doi.org/10.1063/1.2048820
22. B. Lucas, W. Oliver, G. Pharr, and J. Loubet, "Time dependent deformation during indentation testing," in *MRS Proceedings*, 1996, p. 233.
23. G. Kermouche, J. Loubet, and J. Bergheau, "Cone indentation of time-dependent materials: The effects of the indentation strain rate," *Mechanics of materials,* vol. 39, pp. 24-38, 2007.
24. Paul Baral, Gaylord Guillonneau, Guillaume Kermouche, Jean-Michel Bergheau, Jean-Luc Loubet. Theoretical and experimental analysis of indentation relaxation test. Journal of Materials Research, 2017, 32 (12), pp.2286-2296. ff10.1557/jmr.2017.203ff .
25. Smerdova, O., Pecora, M. & Gigliotti, M. Cyclic indentation of polymers: Instantaneous elastic modulus from reloading, energy analysis, and cyclic creep. *Journal of Materials Research* **34**, 3688–3698 (2019). https://doi.org/10.1557/jmr.2019.289

26. Bulychev, S.I., Alekhin, V.P., Shorshorov, M.Kh., Ternovskij, A.P., & Shnyrev, G.D. (1975). Determination of Young modulus by the hardness indentation diagram. Zavodskaya Laboratoriya, 41(9), 1137-1140.
27. Oliver, W.C., Pharr, G.M. Measurement of hardness and elastic modulus by instrumented indentation: Advances in understanding and refinements to methodology. Journal of Materials Research 19, 3–20 (2004). https://doi.org/10.1557/jmr.2004.19.1.3
28. M. Hardiman, T.J. Vaughan, C.T. McCarthy, The effects of pile-up, viscoelasticity and hydrostatic stress on polymer matrix nanoindentation, Polymer Testing, Volume 52, 2016, Pages 157-166, https://doi.org/10.1016/j.polymertesting.2016.04.003.
29. Guozheng Kang, Ratchetting: Recent progresses in phenomenon observation, constitutive modeling and application, International Journal of Fatigue, Volume 30, Issue 8, 2008, Pages 1448-1472, https://doi.org/10.1016/j.ijfatigue.2007.10.002.
30. Thierry Barriere, Xavier Gabrion, Sami Holopainen, Jarno Jokinen, Testing and analysis of solid polymers under large monotonic and long-term cyclic deformation, International Journal of Plasticity, Volume 135, 2020, 102781, https://doi.org/10.1016/j.ijplas.2020.102781.
31. Song Thanh Thao Nguyen, Sylvie Castagnet, Jean-Claude Grandidier, Nonlinear viscoelastic contribution to the cyclic accommodation of high density polyethylene in tension: Experiments and modeling, International Journal of Fatigue, Volume 55, 2013, Pages 166-177, https://doi.org/10.1016/j.ijfatigue.2013.06.013.